Geophys. J. Int. (2004) **156,** 115–128 doi: 10.1111/j.1365-246X.2004.02119.x

Deep reflection surveying in central Tibet: lower-crustal layering and crustal flow

Andrew R. Ross,[1,*] Larry D. Brown,[1] Passakorn Pananont,[1] K. D. Nelson,[2] Simon Klemperer,[3] Seth Haines,[3] Zhao Wenjin[4] and Guo Jingru[4]

[1] *Institute for the Study of the Continents, Snee Hall, Cornell University, Ithaca NY* 14853, *USA*
[2] *Department of Earth Sciences, Heroy Geology Laboratory, Syracuse University, Syracuse, New York* 67544, *USA*
[3] *Department of Geophysics, Mitchell Building, Stanford University, Stanford, CA* 94305-2255, *USA*
[4] *Chinese Academy of Geological Sciences, Beijing, China*

Accepted 2003 September 8. Received 2003 August 5; in original form 2002 May 23

SUMMARY

In the summer of 1998, a series of multichannel, deep seismic reflection tests were conducted in central Tibet around 89°E as part of the third phase of Project INDEPTH, a multidisciplinary study of the structure of the core of the Tibetan Plateau. Short seismic reflection sections from four locations spanning the Jurassic Banggong–Nujiang Suture show several features: thin (<2 km), sedimentary cover sequences; an unreflective upper crust down to approximately 25 km depth; strongly reflective lower crust down to 65 km depth (22 s traveltime) and a distinct change in seismic character from layered reflectivity to unreflective that we interpret as marking the reflection Moho. These profiles are unlike those in parts of the Yadong–Gulu Rift to the south where few deep reflections exist and reflection profiles are dominated by high-amplitude reflection bright-spots at 6 s which have been interpreted as fluid bodies, either water or magma. Analyses of seismic amplitude decay on individual shot records confirm source-generated energy at traveltimes beyond 22 s, thus indicating that the change in reflection character at the Moho is not the result of a loss of signal penetration. The depths to the top and bottom of the lower-crustal reflectivity match both a mid-crustal velocity increase and the Moho determined for this area from refraction profiling. Lower-crustal reflectivity is consistent with current ductile deformation as suggested by models for middle and lower-crustal flow in Tibet. However, Cretaceous-age magmatic intrusions may explain at least part of the observed reflectivity.

Key words: continental deformation, crustal structure, explosion seismology, Moho discontinuity, seismic reflection.

INTRODUCTION

In this paper, we present seismic reflection data collected during phase III of Project INDEPTH (INternational DEep Profiling of Tibet and the Himalayas), a multidisciplinary, multinational initiative to investigate the crust and upper-mantle of southern Tibet. Previous INDEPTH seismic reflection studies in Tibet were carried out across the Tethyan Himalaya and Lhasa Block of the southern Tibetan Plateau. The results from the INDEPTH I and II seismic transects are discussed in several publications (Zhao *et al.* 1993; Brown *et al.* 1996; Makovsky *et al.* 1996, 1999; Nelson *et al.* 1996; Alsdorf *et al.* 1998; Cogan *et al.* 1998; Hauck *et al.* 1998; Makovsky & Klemperer 1999; Ross *et al.* 2003). The most significant results from the reflection profiling element of INDEPTH thus far are: (1) a reflection Moho at 23 s traveltime, or 75 km depth, at the southern end of the profile (Zhao *et al.* 1993); (2) a prominent reflection marking the Main Himalayan Thrust, the active decollement along which the Indian Plate is underthrusting Asia, on INDEPTH surveys south of the Indus–Yarlung Suture (Zhao *et al.* 1993; Hauck *et al.* 1998); and (3) a series of extremely high-amplitude reflections or 'bright-spots' (Brown *et al.* 1996; Alsdorf *et al.* 1998; Ross *et al.* 2003) at 15 km depth beneath the northern portion of the INDEPTH II profile. These bright-spots are interpreted as fluids and are most likely indicative of the existence of melt beneath at least this portion of southern Tibet (Ross *et al.* 2003). Few significant reflections are observed below the level of the bright-spots. Moreover, the existence of extremely high conductivities (Chen *et al.* 1996) and low seismic velocities (Yuan *et al.* 1997) below the bright-spot zone has fuelled speculation that the entire middle crust of southern Tibet may be partially molten (Nelson *et al.* 1996). Analysis and modelling of

*Now at: Geological Institute, University of Copenhagen, Øster Voldgade 10, Copenhagen, DK 1350, Denmark.

MAGSAT magnetic anomalies have lent support to the suggestion that such melting may be widespread across the plateau (Alsdorf & Nelson 1999).

However, the earlier INDEPTH observations were all made within a discrete zone of active rifting, the Yadong–Gulu Rift system, raising concerns that the seismic character observed and any fluids or partial melting may be a local effect associated with specific extensional structures. In order to determine the extent of partial melting beyond the southern Tibetan rifts and thus test the hypothesis that such melting is responsible for plateau uplift as a whole (Nelson *et al.* 1996), the third stage of INDEPTH, INDEPTH III, was centred on the Late Jurassic age Banggong–Nujiang Suture (Kidd *et al.* 1988), the boundary between the Qiangtang and Lhasa blocks, two major constituent blocks of the Tibetan Plateau (Fig. 1) in an area that lies outside the rift system. In addition to a surface suture, this region spans what has been suggested to be a mantle suture between India and Asia with a change from high-velocity upper-mantle material to the south and lower velocity, attenuating upper mantle to the north (McNamara *et al.* 1997; Owens & Zandt 1997; Huang *et al.* 2000).

The INDEPTH III project is composed of a number of different geophysical (active and passive seismology and magnetotelluric profiling) and geological components (Fig. 1). The core of the INDEPTH III seismic experiment was an array of 57 broad-band and intermediate-period, three-component seismographs (mostly Streckeisen STS-2) deployed primarily along a NNW–SSE profile designed to record teleseismic earthquakes for use in tomographic

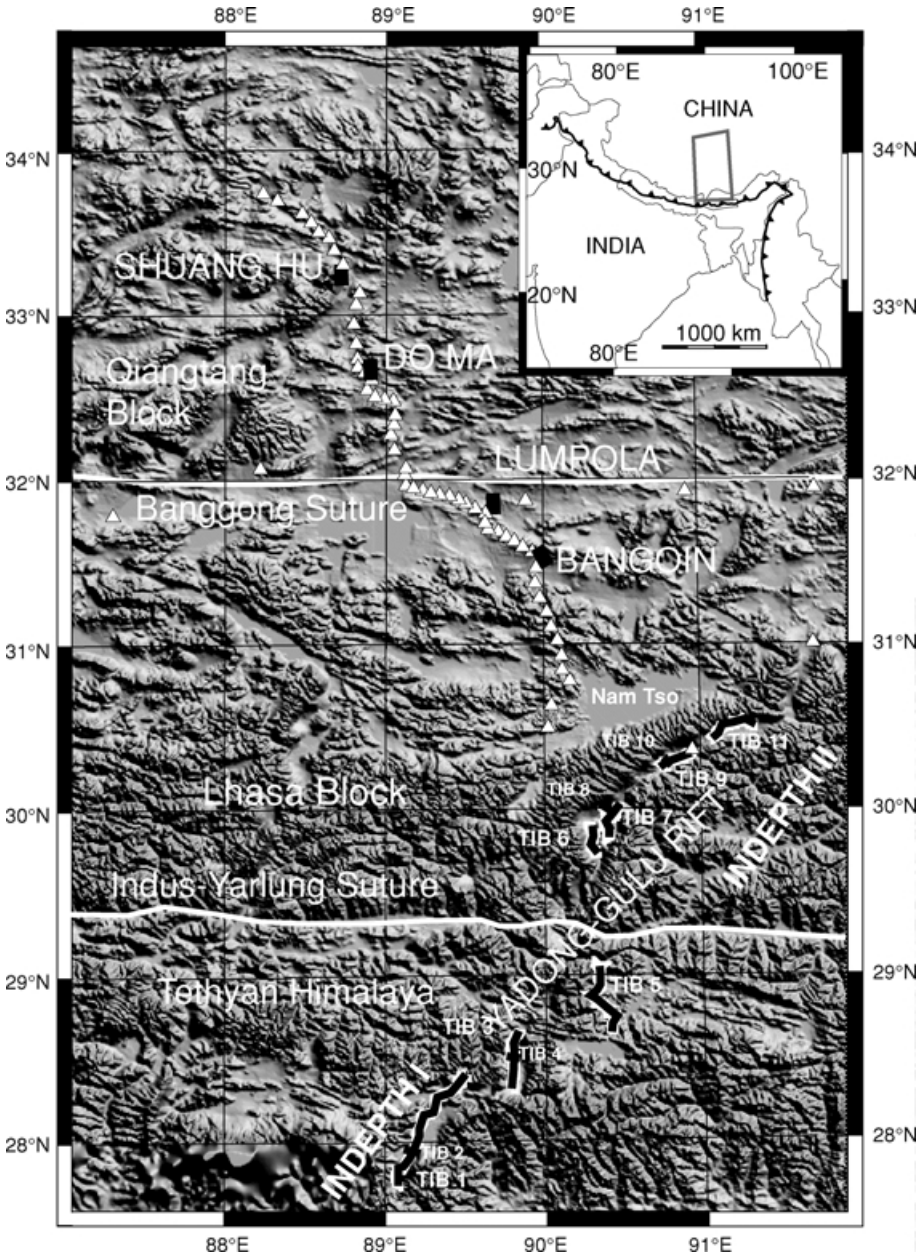

Figure 1. Topographic map of central Tibet between 87°E and 92°E longitude and 27.5°N and 34.5°N latitude. The solid black lines show the locations of INDEPTH seismic reflection profiles. INDEPTH I and II profiles are labelled. INDEPTH III profiles are identified by the names in capitals. The white triangles show the locations of the INDEPTH III temporary seismic deployment. The solid white lines identify the approximate locations of the two sutures in this region. Other tectonic features mentioned in the text are labelled.

and receiver function analysis of crustal and upper-mantle structure. Additionally, 11 large (up to 2000 kg) chemical explosions were detonated for recording by this array to provide a reversed refraction profile and hence gross crustal velocity structure (Zhao *et al.* 2001). Funding limitations made it impossible to have both full-scale reflection profiling and the planned broad-band deployment. However, it was possible to acquire a series of five short common mid-point (CMP) test lines at widely spaced locations along the main transect route (Fig. 1). These tests were designed to determine whether or not deep reflection profiling was viable in this region, given concerns about signal penetration raised by the lack of deep reflections on the reflection lines in the northern part of the Yadong–Gulu Rift. The line locations were chosen in order to sample as wide a range of geology and hence recording conditions as possible, both north and south of the Banggong–Nujiang Suture. Three temporary deployments of refraction seismographs also recorded the reflection and refraction shots to provide three component data at offsets of up to 30 km and velocity information down to 25 km depth (Haines *et al.* 2003). We concentrate on the reflection experiment in this paper, reporting the first results of crustal-scale multichannel recording in the central Tibetan Plateau.

ACQUISITION AND PROCESSING

Four reflection lines (near the small towns of Bangoin, Lumpola, Do Ma and Shuang Hu) and one short crossline (at Shuang Hu) were acquired from 1998 mid-July to early August. The first two locations lie to the south of the Banggong–Nujiang Suture within the Lhasa block, while the latter two sample the Qiangtang terrane. The terrain, although containing occasional regions of high relief, is mostly rolling hills with numerous, shallow, ephemeral lakes. Each of these lines was oriented approximately NW–SE, was located in a relatively flat lying area (Fig. 1) and had broadly similar acquisition geometries (although local difficulties in drilling suitable shot holes caused variations from the nominal source–receiver geometry for each line). Around 160 dynamite shots were recorded at variable offsets up to 15.5 km into a fixed-location 60 channel recording system with stations spaced 32.0 m apart for the Bangoin line and at 31.25 m intervals for the other three recording locations. Fixing the geophone locations resulted in greatly reduced shooting time (typically 1–1$\frac{1}{2}$ d per deployment) and required significantly less manpower than a roll-along scheme would have required, but resulted in reduced fold for deep reflections and no coverage for shallow structures at the far ends of the profiles. Data was recorded with the PASSCAL 60 channel Geometrics system to a record length of 63 s. Single vertical component geophones (Mark Products L-28) were used. These geophones have a dominant frequency of 4.5 Hz as opposed to typical reflection profiling geophones with 10 Hz dominant frequencies, which should aid in detecting deep or low-frequency reflections. No geophone arrays were utilized. Small shots of 6 kg were detonated close to the spread with larger 50 kg shots deployed at larger offsets in an attempt to minimize the effects of ground roll. Additional very small (2 kg) shots were detonated at either end of each geophone spread to allow for improved definition of shallow structure and receiver statics.

The general quality of the data decreases from south to north and also with time (the lines were acquired in a south to north progression). The Bangoin line has the best and the final Shuang Hu crossline the worst data quality. The reason for this difference is not entirely clear. However, the weather and ground conditions deteriorated throughout an unusually wet summer in central Tibet and may have played a role in the degradation of the data quality. Furthermore, trigger timing was a problem for the lines at Do Ma (20 per cent of shots had problems), Shuang Hu (20 per cent) and the Shuang Hu crossline (100 per cent). This was due to failures of the GPS master clock connected to the recording system. We corrected for these timing problems (which could be as much as several seconds and were typically random i.e. both early and late triggering) by using a single 1-D velocity model for each line to estimate shot origin times for questionable records. Of course, crustal reflectivity itself may have changed, but on each line (except the Shuang Hu crossline) at least one shot shows evidence of deep reflectivity.

All the data were processed with the ProMAX seismic processing package. The data processing flow used to produce the stacked sections shown here is given in Table 1. Ground roll was visible on

Table 1. Processing Flow for INDEPTH III reflection data.

Operation	Comments
Geometry application	Straight line geometry. CDP spacing 15.625 m (16 m for Bangoin line)
Trace DC removal	Mean value
Spike and noise burst editing	High and low pass.
Top mutes and trace kills	
Surgical mutes	Reflected refractions
Elevation statics	Datum at mean elevation of spread. Replacement velocity = 2.5 km s^{-1}
Hand statics	Removed 600 ms systematic time delay plus timing corrections based on traveltime curves for Do Ma, Shuang Hu and crossline
Residual statics	Correlation autostatics. Maximum static = 25 ms
Bandpass filter	Ormsby minimum phase frequency domain filter : 9-12-30-35 Hz. for 0–7 s and 4-7-30-35 from 7 s to the end of the record
Normal moveout correction	Velocities from constant velocity stacks, refraction analysis and big shots
F-X deconvolution	Applied over 20 trace window
AGC	2000 ms window for displayed data
Ensemble balancing	
Mean stack	Trace fold = 8
F-K filter	Remove air waves
F-X deconvolution	Applied over 50 trace window.
Bandpass filter	
Depth conversion	Using refraction velocities from Zhao *et al.* (2001)
Display	

most shots, undoubtedly exacerbated by the use of single geophones as opposed to geophone arrays. However, the use of a time-varying bandpass frequency filter (ramping at the low-cut from 9 to 12 Hz for 0–7 s and 4–7 Hz for longer times) for the shallow section and at depth proved effective in eliminating ground roll, while preserving low frequencies for deeper reflections compared with the peak frequency response of the geophones (4.5 Hz). High-frequency noise (above 35 Hz) was also a problem. This noise was wind generated since the weather conditions during the summer of 1998 included frequent thunderstorms and our lines were deployed in flat areas with little shelter. This high-frequency noise was removed by excluding frequencies greater than 35 Hz.

REFLECTION CHARACTER OF CENTRAL TIBET

The results of the processing of the four main lines are shown in Fig. 2. The Shuang Hu crossline is so dominated by noise (a windstorm occurred at the time of recording) that no reflections were identified and we do not show it here. The lines are shown unmigrated. Their short length (<7.5 km) generates such significant migration artefacts (e.g. Warner 1987) that the results are not interpretable. However, the dips observed in the data are sufficiently low (<10°) that migration should not significantly effect the locations or dips of any of the reflections observed.

There are several features observed on these lines: (1) a generally non-reflective region from approximately 3 to 25 km depth (1–9 s traveltime); (2) a highly reflective region from 25 km down to around 65 km (9 s down to approximately 20–22 s traveltime); and (3) a non-reflective region from deeper than 65 km (22 s TWT) to the end of the records. The insets in Fig. 3 illustrate each of these features on the Bangoin, Lumpola and Do Ma lines. In addition, the Bangoin line has a clear sedimentary basin extending down to 1.5 s traveltime (Fig. 4).

The first of the reflectivity changes occurs at 9 s TWT on the Bangoin line, at 8 s on the Lumpola line and somewhere between 7 and 9 s on the Do Ma line (Figs 3d–f). The reflectivity change is most pronounced on the Bangoin line. On the other two lines it is much more subdued, though still visible as a distinct change on the Lumpola line. On the Do Ma line, the change is less clear coinciding with an increase in reflectivity over a 2 s window as opposed to a sharp change. The reflectivity increase corresponds to a change not only in reflection amplitude and density (i.e. number of reflections), but also a change in the frequency content (enhanced frequencies at around a peak of 20 Hz as opposed to 10 Hz above and below this zone) and reflection length (from approximately 3 to 4 CMPs, or 50–60 m, for the few reflections observed, to over 30 CMPs or 500–600 m (Figs 3a and 5)). This change cannot be the result of changes in the Fresnel zone radius. At 20 km depth for a crustal velocity of 6.1 km s^{-1} (Zhao *et al.* 2001) and a frequency of

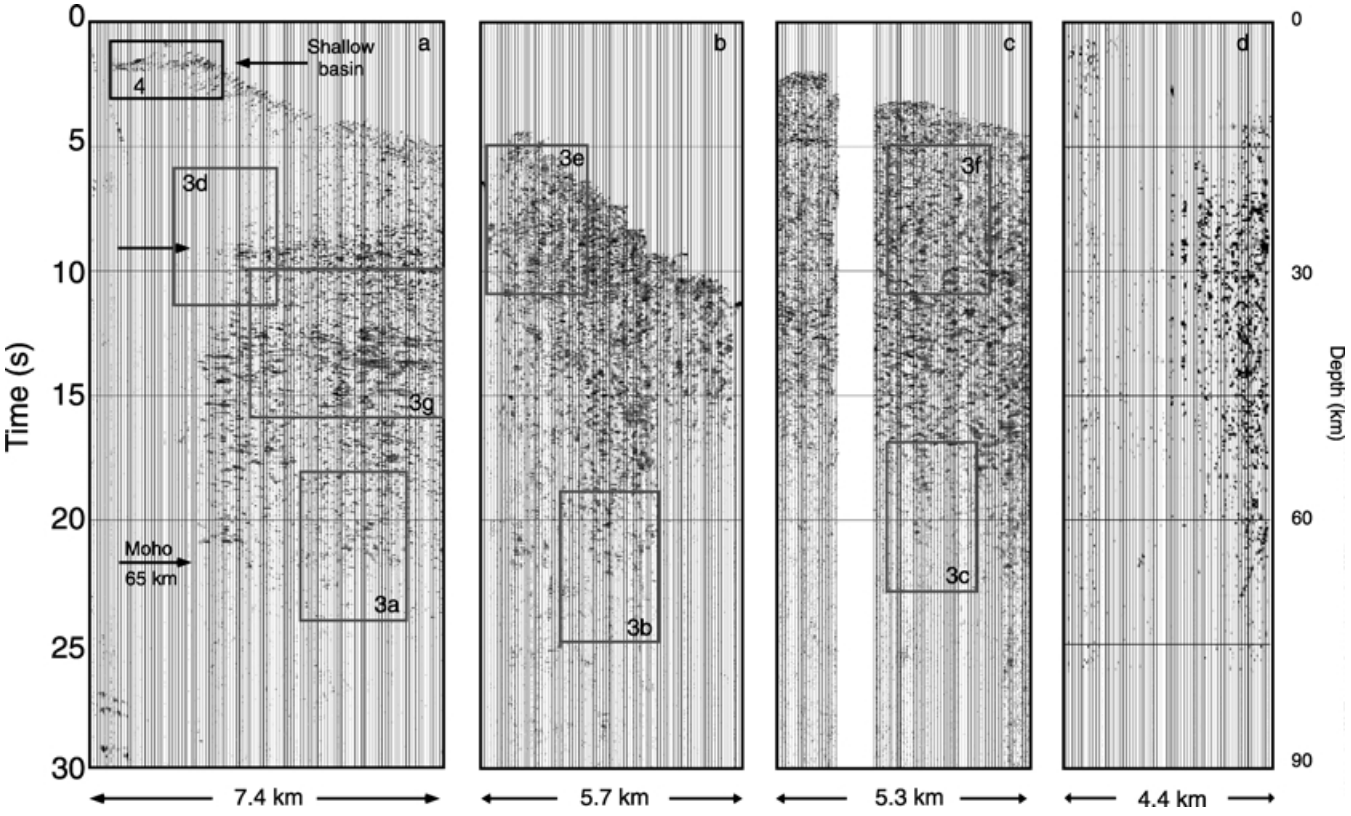

Figure 2. Unmigrated stacks of INDEPTH III CMP lines, Bangoin (a), Lumpola (b), Do Ma (c) and Shuang Hu (d). The horizontal exaggeration is 6:1. Recordings were made to 63 s but only 30 s are shown here. The CMP spacing is 16 m for Bangoin and 15.625 m for the other lines. The boxes indicate locations of details shown in Figs 3 and 4. The three southern lines show considerable mid-crustal reflectivity with a clear Moho cut-off on the Bangoin line and in the centre of the Lumpola line and a much more poorly defined cut-off on the Do Ma line. On both the Bangoin and Lumpola lines the near offset shots were only 6 kg, explaining the low amplitudes at the southern end of the Bangoin line. On the Do Ma line there was a gap in coverage in the middle of the line. The Shuang Hu line is generally of poor quality but shows some mid-crustal reflectivity.

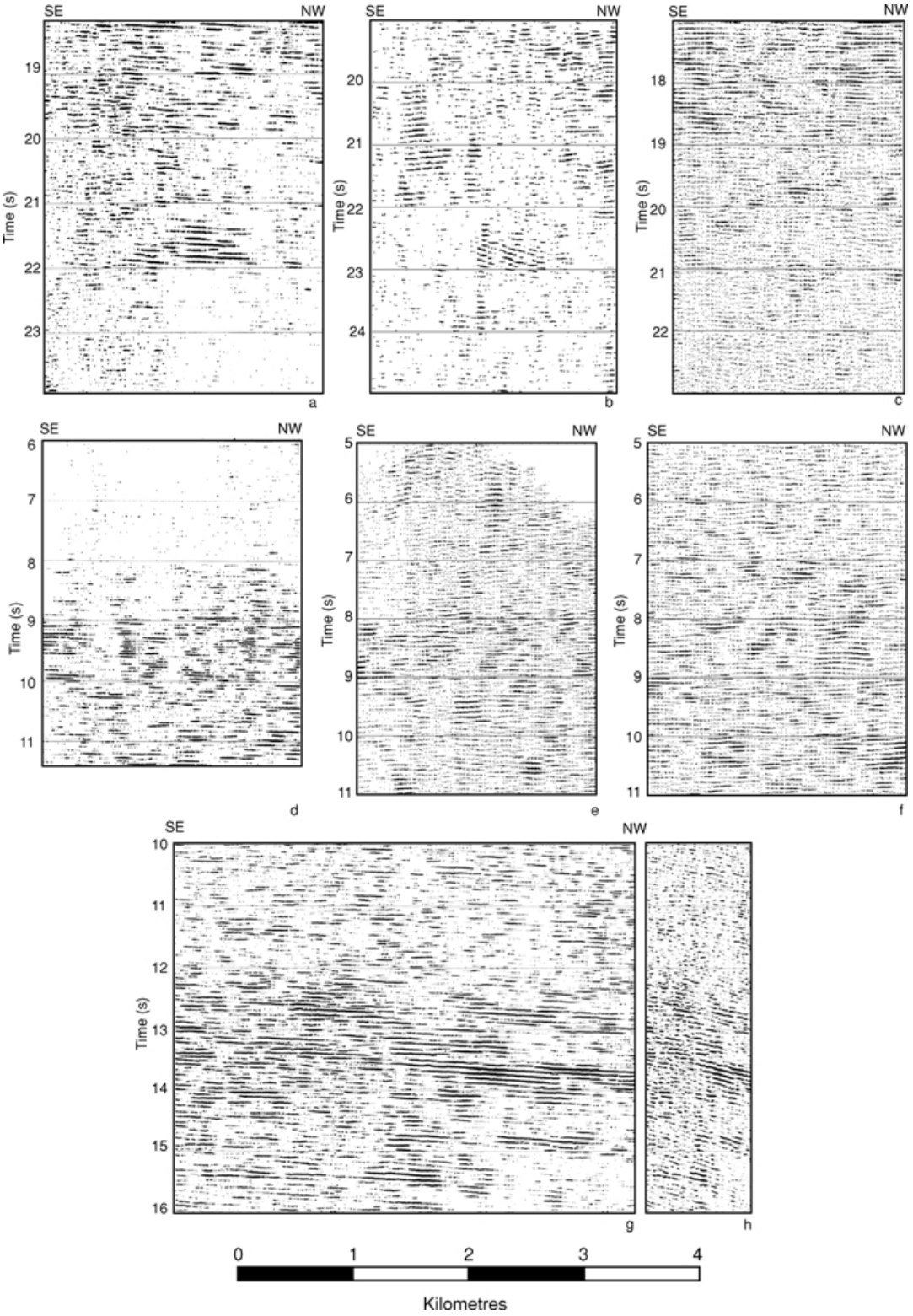

Figure 3. Details of the INDEPTH III reflection profiles. The horizontal exaggeration is 375 per cent and all insets except for the last are shown at the same horizontal scale. The Moho reflectivity cut-off is clear at 22 s TWT on the Bangoin line (a). It is more pronounced for the Bangoin line than for Lumpola (b), but a cut-off is visible at the same TWT of 22 s. For the Do Ma line (c) the reflectivity cut-off is much less clear and happens at around 21 s TWT. This may reflect signal penetration issues (see Fig. 6) or a shallower depth to the Moho. The depth to the Moho cut-off at 22 s is 63 km. The mid-crustal reflectivity starts at 9 s TWT on the Bangoin line (d) with a transition from a region with virtually no reflectivity above this traveltime to strong reflectivity below. A weaker increase of reflectivity is visible on the Lumpola line at around 8 s TWT (e). On the Do Ma line (f) the upper boundary is not a sharp increase in reflectivity, but a more gradual one. (g) A close up of the strongly reflective interval at 13 s traveltime on the Bangoin line. The continuity of the reflectivity increases noticeably between 13 and 15 s when compared with the reflectivity above 12 s. This corresponds to a depth of 40 km. (h) Same time interval as the inset in (g) at 1:1 scaling showing the dip of this reflectivity to the NW.

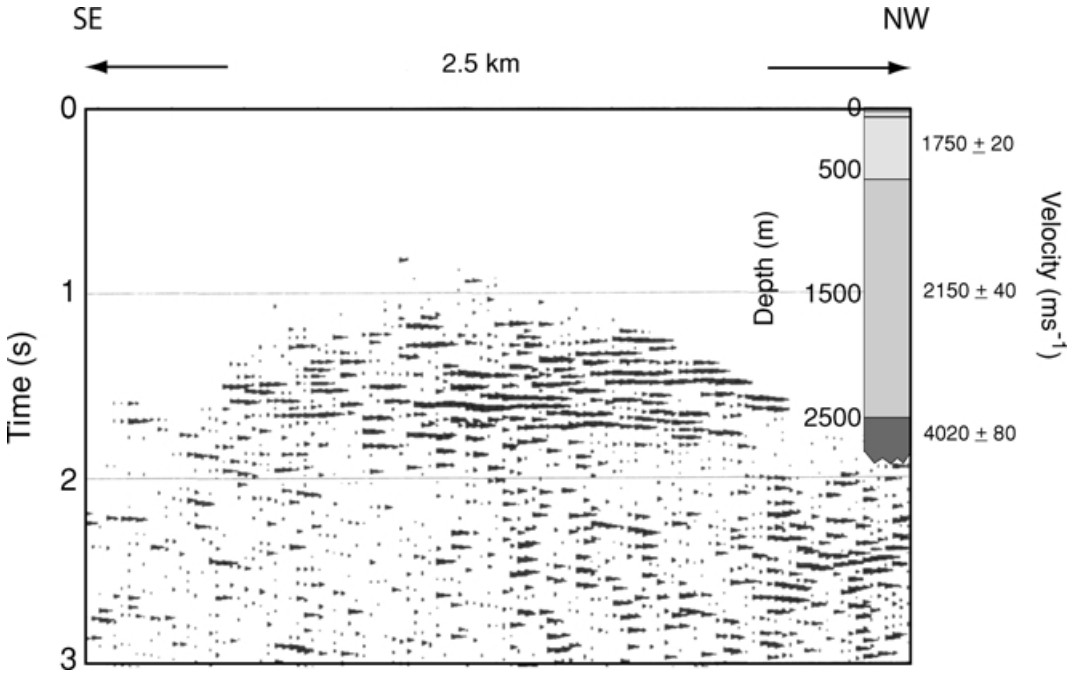

Figure 4. A close up view of the basin on the Bangoin line. Linear subhorizontal reflectivity extends down to almost 2 s. Below this the reflectivity has an increased dip suggesting an unconformity at this depth and that the base of the subhorizontal reflectivity corresponds to the bottom of a recent sedimentary basin. This is confirmed by 1-D refraction analysis of the first arrival velocities (shown to the right of the reflection data), which show a significant jump from 2150 to 4020 m s^{-1} at a depth corresponding to the reflectivity change after depth conversion. Velocities of 2150 m s^{-1} are consistent with velocities found in young basins (Sheriff & Geldart 1987).

20 Hz, the Fresnel zone is 1.23 km. For a velocity of 6.4 km s^{-1} and a frequency of 20 Hz it is 1.27 km. This is not a large change in size and cannot explain the change in reflectivity.

This region of increased length and density of reflectors continues down to 22 s traveltime for the Bangoin line, corresponding to around 62–65 km depth. At this point, the reflectivity abruptly stops (Figs 3a and 5). For lines other than Bangoin, the reflectivity cut-off is not as clear (Figs 3b, c, 2b–d) and for Do Ma occurs at a shorter traveltime of 21 s (Fig. 3c). Additionally, the lines other than Bangoin have much lower data quality and much greater variability between individual shots: they show reflectivity but both the upper and lower reflectivity cut-offs are not as clear. Again, Fresnel zone size cannot explain the reflectivity cut-off. For a frequency of 20 Hz and a velocity of 7.3 km s^{-1} at 65 km, the Fresnel zone radius is 2.44 km. For a velocity of 8.0 km s^{-1} at 65 km, the Fresnel zone radius is 2.55 km.

Converting our data to depth using a refraction velocity model derived from the shots recorded by the INDEPTH III seismic array (Zhao *et al.* 2001) gives a depth to the lower reflectivity cut-off of 62–65 km (Figs 2 and 3). The depth to the refraction Moho at Bangoin has been estimated by Zhao *et al.* (2001) to be 66 km. Thus we interpret the change from a reflective to a non-reflective character at 22 s traveltime as the reflection Moho. This is shallower than other previously published Moho depths for this area of central Tibet; 74 km (Owens & Zandt 1997); 70 km (Sapin *et al.* 1985) and 70 km (Kong *et al.* 1996). However, these surveys do not sample exactly the same region of the crust indicating some possible along strike variations in Moho thickness. The slightly shallower cut-off at Do Ma (60 km) may reflect signal penetration problems but may also reflect the slight shallowing of the Moho in the northern part of the INDEPTH III profile reported by Zhao *et al.* (2001).

Although there is no discrete Moho reflection, the reflectivity cut-off occurs over a narrow depth range. This reflectivity cut-off is typical of the Moho in other areas such as the Southern Urals and the Trans-Hudson Orogen (e.g. Steer *et al.* 1998) where changes in reflectivity are also interpreted to indicate the crust–mantle boundary. The upper-mantle is unreflective with no evidence of any discontinuities or fabrics. The lack of a prominent Moho reflection suggests that there has not been any recent magmatic underplating of the crust (Klemperer *et al.* 1986). It also suggests that any 'detachment' at the Moho due to speculated underthrusting of Indian upper-mantle beneath Asia is unreflective (Barazangi & Ni 1982). However, the very limited length of our profiles is obviously not well suited to deducing the regional characteristics of the Moho.

One particular concern in interpreting both the Moho and an unreflective mantle is whether the shot energy is penetrating to these traveltimes: the change in reflectivity at the Moho could simply be an energy penetration cut-off. However, amplitude decay curves for typical shot gathers for each of the INDEPTH III lines (Fig. 6a) clearly show energy penetrating well below 22 s (our interpreted Moho traveltime at Bangoin) suggesting that there is a true change in reflectivity at this traveltime and not a penetration cut-off. However, the Do Ma line has much less energy at longer traveltimes which might explain the much poorer quality at depth of this line and also the cessation of reflectivity at traveltimes less than 22 s. The relative signal penetration of shots of varying size is shown in Fig. 6(b) for the Bangoin line. The 50 kg shots produce the highest amplitudes and the best apparent signal penetration, and the 2 kg shots produce the worst. However, it is of note that even for the 2 kg shots the amplitude does not decay to ambient noise levels until 16 s traveltime. The 6 kg shot cut-off does not decay until 26 s traveltime, while the 50 kg shot penetrates until 36 s traveltime. In fact, weak, but identifiable

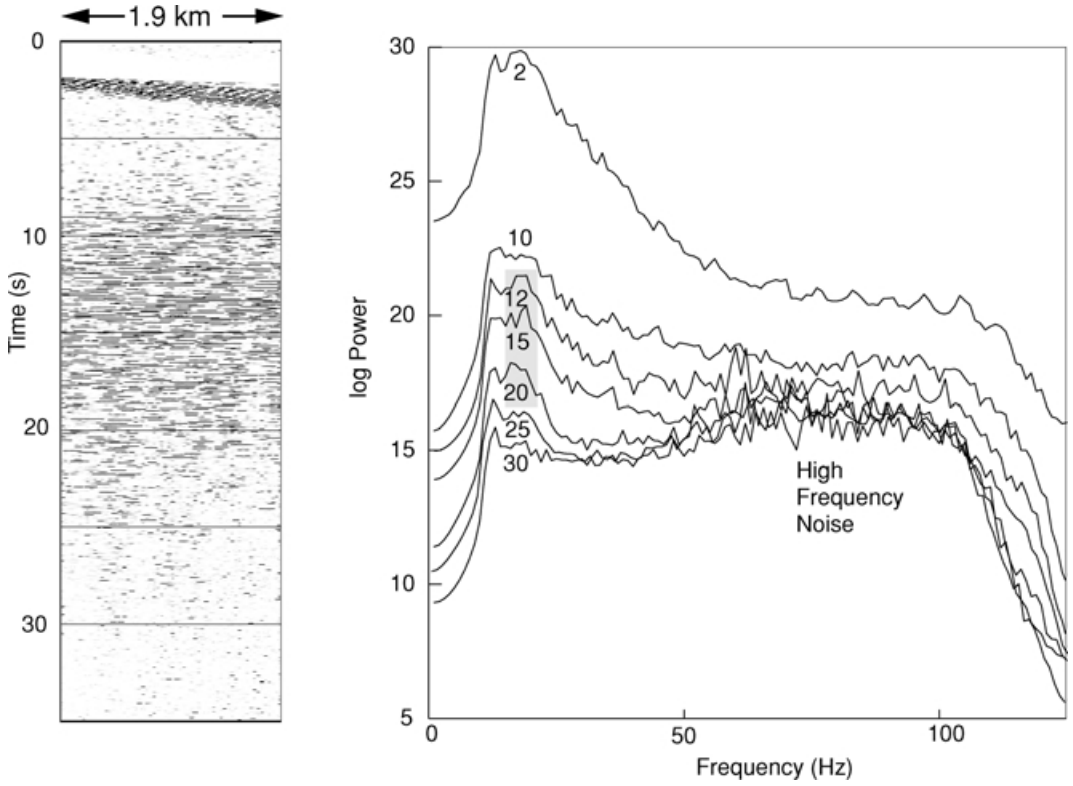

Figure 5. Power spectra for Bangoin shot number 424. Numbers in power spectra correspond to times of 1 s windows used to produce the power spectra. The power clearly decreases below 20 s, with high-frequency noise, most likely wind generated, dominating the records at later traveltimes. A frequency peak near 20 Hz (grey box) corresponds to the mid-crustal reflectivity on the shot at these traveltimes.

reflections at Moho depths are seen on the 6 kg shots at Bangoin. However, the reflection amplitudes for traveltimes beyond 10 s on the 50 kg shots are much greater than those on the 6 kg shots and only the 6 kg shots at Bangoin have identifiable deep reflections. The slope of the amplitude decay in central Tibet compares well with INDEPTH I in the Tethyan Himalaya, where a clear, sharp Moho reflection was observed at 23 s traveltime (Fig. 6c) suggesting that seismic penetration in central Tibet is as good as in the Himalayas, where the deepest reflection Moho in the world was observed (Hauck *et al.* 1998).

In the middle crust, the short length of our profiles and our spread length (1.95 km) does not give much control on deep reflector dip and structures. The Fresnel zone is larger than our spread length for traveltimes of more than approximately 7 s. Hence, interpreting more than the existence of reflectivity is problematic, particularly with respect to dips of individual reflectors. For example it is possible that we are seeing diffractions from small-scale heterogeneities that give the impression of being linear reflectivity (Gibson & Levander 1990). However, there is clearly a change in reflection character at the top and the bottom of the reflective region which indicates a difference in the physical properties above and below. Furthermore, at 12.5 s traveltime on the Bangoin line, a zone of reflectivity is visible across the entire line with higher amplitudes than the surrounding reflections (Fig. 3g). This reflection package appears to dip to the northwest at approximately 10° suggesting a true location slightly to the southeast of our line (Fig. 3h). The short line length makes it virtually impossible to link this feature to surface geology. The Banggong–Nujiang Suture is interpreted to be a north-dipping structure (Coward *et al.* 1988). However, its surface trace lies 30 km to the north of the Bangoin line. It is thus unlikely that this reflective package, if it is a structure, is an image of the suture unless the suture at depth is offset with respect to its surface trace.

Some independent confirmation of the significance of the reflectivity observed in our data comes from refraction analysis of the large shots (Zhao *et al.* 2001). They report two separate intracrustal reflectors that they observe on all the good large shot recordings. These interfaces extend along the entire length of the INDEPTH III profile. The first of these reflections comes from an interface that has a similar depth to the onset of reflectivity on the Bangoin reflection line at 9 s TWT or 27 km. This reflection corresponds to a jump in velocity from 6.1 to 6.5 km s^{-1} in the velocity model derived from the large shot record sections. The second of the intracrustal reflectors has a depth of 45 km that may correspond to a package of higher amplitude reflectivity at 13 s on the Bangoin line (Fig. 3c). The velocity jump at this boundary is much smaller at this location (0.1 km s^{-1}). Both of these boundaries are shallower at the northern end of the big shot refraction profile than the southern end by approximately 10 km: from 32 km depth at the southern end of the profile rising to 19 km at the northern end for the uppermost boundary. This shallowing of the upper boundary is reflected in the shallowing of the upper reflectivity cut-off on the Lumpola and Do Ma lines with the Lumpola line fitting the approximately 25 km depth to this boundary at its location. The deeper boundary rises from 46 km depth in the south to 31 km in the north but there is no indication of it on the lines other than Bangoin. The correspondence of the onset of layered reflectivity with an intracrustal wide-angle reflection and a velocity increase adds considerable confidence to our interpretation of a significant change in the crust at this depth. The velocity change of 0.4 km s^{-1} at the top boundary would correspond to a reflection coefficient of 0.03, which would be expected

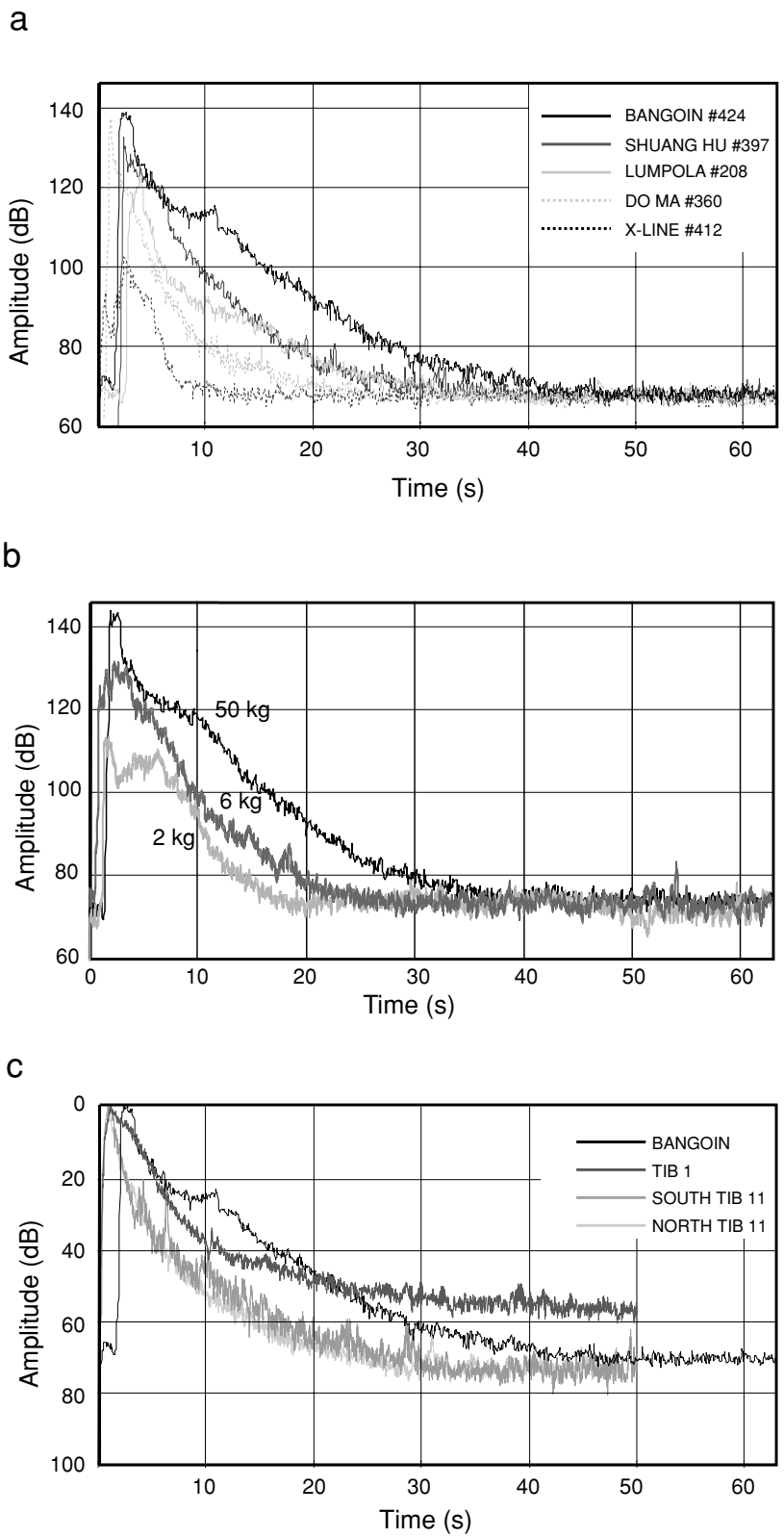

Figure 6. (a) Amplitude decay curves for representative shots on the INDEPTH III lines. The Bangoin line clearly has significantly higher amplitudes to greater traveltimes than the other lines. (b) Variation in amplitude decay for different shot sizes from the INDEPTH III line Bangoin. Shots of 2, 6 and 50 kg are plotted together. The 50 kg shot has the best signal penetration, down to traveltimes beyond 36 s. However, even the 2 kg shot shows some signal penetration down to traveltimes beyond 10 s. (c) Comparison of amplitude decay curves for INDEPTH I (TIB 1), INDEPTH II (TIB 11) and INDEPTH III (Bangoin) displayed as dB down from the maximum amplitude to account for differences in amplitudes between surveys acquired with different recording systems. The signal penetration for Bangoin and TIB 1 is comparable. For TIB 11, the signal penetration is similar for both shots shown. However, their reflection character is different.

to produce an observable reflection. This may be a compositional boundary given the large increase in velocity at this depth identified by Zhao *et al.* (2001).

The large number of reflection shots allows us to determine the 1-D shallow velocity structure for our lines from the first arrivals. All the lines except Bangoin and Shuang Hu have virtually no recent sediments with velocities of over 4000 m s^{-1} at shallow depths and velocities of over 5000 m s^{-1} at around 1 km depth. A thin 500 m basin exists at Shuang Hu, consistent with its location in a small graben. However, for Bangoin, velocities of less than 2200 m s^{-1} exist down to 2.5 km suggesting the existence of a reasonably deep basin at this location. Fig. 4 shows this basin on the reflection data. A depth conversion of the section shows that the base of the reflectivity approximately corresponds to the bottom of the basin indicating that the shallow 'basement' in this region is unreflective: presumably the Bangoin granite, which outcrops a few kilometres to the south of the profile location. The results of inversion of the first arrivals confirm the existence of this low-velocity basin beneath the Bangoin line (Haines *et al.* 2003). The extremely low seismic velocity in this basin suggests that it is filled with poorly consolidated and probably very young sediments.

COMPARISON WITH INDEPTH I AND II: AMPLITUDE DECAY AND REFLECTIVITY

The most obvious distinction between the multichannel profiles on INDEPTH I/II and INDEPTH III is the lack of the anomalously high-amplitude reflections, or bright-spots, found at 15 km on the INDEPTH II profiles (Brown *et al.* 1996), but not observed at any depth on the INDEPTH III lines. These reflections are interpreted as being from fluids in the middle crust. The lack of strong reflectors on the INDEPTH III lines, however, does not entirely rule out the existence of fluids in the crust outside the Yadong–Gulu Rift zone. The lengths of the INDEPTH III reflection profiles are very short and sample a very small region of the central plateau: it is quite possible that high-amplitude reflectors exist at locations where we did not acquire surveys. The INDEPTH II lines cover a distance of over 200 km compared with the much shorter distance of the INDEPTH III lines. Even including the temporary deployments in INDEPTH III (Haines *et al.* 2003), which, unlike the wide-angle deployment for INDEPTH II (Makovsky & Klemperer 1999), show no bright wide-angle reflections, the total distance with data coverage is approximately only a third of that for INDEPTH II. In the Yadong–Gulu Rift zone both a low-velocity zone (Yuan *et al.* 1997) and a magnetotelluric high conductivity layer (Chen *et al.* 1996) correlate with the bright-spot reflections (Brown *et al.* 1996; Makovsky & Klemperer 1999; Ross *et al.* 2003). Satellite magnetic data and a determination of the depth to the Curie isotherm suggest that melt could underlie the whole plateau (Alsdorf & Nelson 1999) below approximately 15 km. This conclusion is supported by Wei *et al.* (2001) who report high conductivity values in the region of the INDEPTH III profiles. The conductivity is an order of magnitude lower than in the rift zone but is still much higher than for normal crust and indicates the presence of melt or aqueous fluids (Wei *et al.* 2001). However, unlike the Yadong–Gulu Rift zone, there is no direct seismic evidence for the presence of melt or water. Surface wave analysis shows no crustal low-velocity zone (Rapine *et al.* 2000). While not ruling out the existence of a low-velocity zone, refraction analysis (Zhao *et al.* 2001) does not require it. Analysis of xenoliths from northern Tibet suggests that the lower crust contains a mostly anhydrous mineralogy with no melt at the present time (Hacker *et al.* 2000). However, magnetotelluric profiling further to the north and east along the Lhasa–Golmud highway shows very high conductivity in that region (Wei *et al.* 2001). These observations led Haines *et al.* (2003) to suggest that there may be melt only east of the Lhasa–Golmud highway in central Tibet north of 31°N and not beneath the INDEPTH III profile.

One indication that there may not be as significant an amount of fluid in the crust in this region is the similarity between the INDEPTH III and the INDEPTH I reflection seismic profiles. A comparison of amplitude decay curves for INDEPTH III with TIB 1 and 11 (Fig. 6c) shows that energy penetration in the regions of central Tibet we sampled is extremely efficient, comparable to that at the southern end of TIB 1, where a Moho reflection is also observed. Not only are there no bright-spots but the crust is again an efficient transmitter of seismic energy.

In order to summarize the variations along the INDEPTH profile, we projected the reflection strength attribute of the stacked seismic data on to a line at 90°E (Fig. 7). Normalizing each trace to account for different shot sizes and acquisition parameters, a clear difference exists between the southern lines, TIB 1–5, the Yangbajain–Damxung lines (TIB 6–11), and the INDEPTH III lines to the north. For TIB 1 the entire crust is reflective, albeit with a drop off of reflectivity in the Indian Plate at the northern end of TIB 1. TIB 3 and 5 show appreciable upper-crustal reflectivity but very little reflectivity in what should be the Indian Plate underthrusting in this region. For TIB 6–11 this situation is more pronounced, with the Yamdrok–Damxung Reflector (YDR) and bright-spots (Brown *et al.* 1996) dominating these lines at 15 km and no deeper reflectivity seen except at the northern end of TIB 11. For the INDEPTH III lines, unreflective upper crust with no YDR equivalent sits above the reflective lower crust. Notably, the change to this lower-crustal reflectivity pattern occurs in the middle of TIB 11, still within the Yadong–Gulu Rift zone. This raises a question concerning the deep character of the crust in the TIB 6–11 segment of the INDEPTH transect. The high reflection coefficients of the YDR bright-spots (0.5 ± 0.2 (Ross *et al.* 2003) and extremely low effective Q together result in very little energy penetrating below the YDR (part of the amplitude decay shown in Fig. 5 may be due to a coda of multiples and converted phases from the bright-spots). The bright-spots and geothermal fluids above the bright-spots may be screening the lower crust: reflective lower crust may exist below. Receiver functions do observe a lower-crustal *P*- to *S*-wave converter above the Moho converter throughout this region (Yuan *et al.* 1997) but this layer lies deeper than the top of the layered lower crust in the INDEPTH III region.

DISCUSSION

The differences in amplitude decay and reflectivity between the central Yadong–Gulu Rift and central Tibet suggest that the crust in these two regions is very different. The reflection seismic properties of the crust in central Tibet have greater similarity to the Himalayas (as seen on-line TIB 1) than the southern parts of the Lhasa Block. However, the lower-crustal reflectivity seen in central Tibet is not observed in the Himalayas. One simple explanation for the different seismic character is that the lower crust of TIB 1 is part of India, whereas the lower crust in central Tibet is not. It suggests that the reflectivity in central Tibet is a result of events ongoing within the plateau or during its formation that do not occur in the Indian Plate. However, an important question is whether the reflectivity we

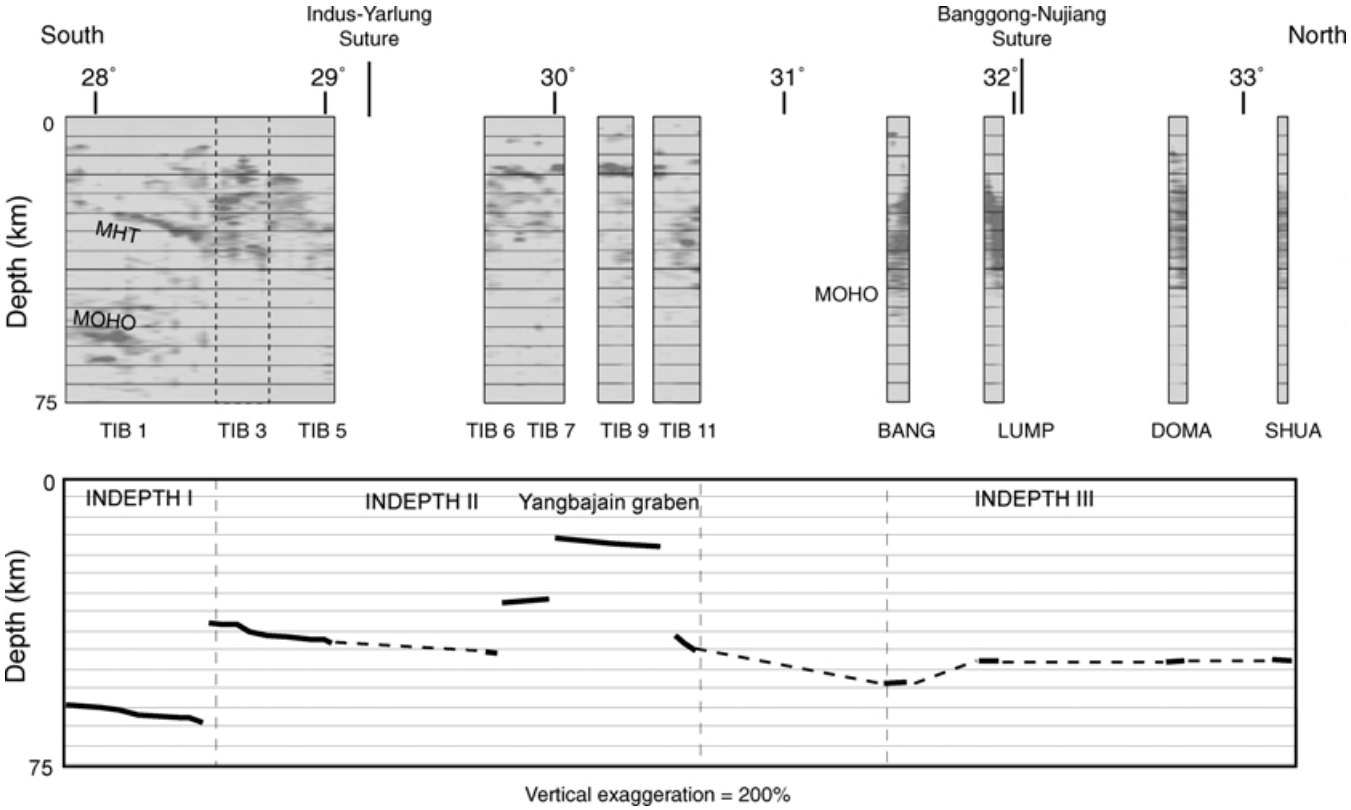

Figure 7. Reflectivity of INDEPTH surveys at approximately longitude 90°E. Clear Moho and MHT (Main Himalayan Thrust) reflections can be seen on TIB 1. TIB 6–11 are dominated by reflectivity around 15 km depth. Starting from the middle of TIB 11, mid-crustal reflectivity is replaced by lower-crustal reflectivity that stops at the Moho. The reflectivity cut-off is shown below the reflection strength plot. Solid lines indicate the regions where we have data. Dashed lines are interpreted.

observe in central Tibet is a modern feature reflecting ongoing processes, a fossilized fabric indicating pre-Himalayan collision crust, or merely the result of very limited sampling of a complex structure giving the illusion of a pervasive fabric in the crust. We cannot discount this last possibility without the acquisition of additional seismic data and so will not discuss it further other than to note that it is a possibility.

Distinctive, enhanced lower-crustal reflectivity has been observed in a number of locations around the world such as the Basin and Range (Allmendinger *et al.* 1987) and western Europe (Matthews & Cheadle 1986). There have been several explanations proposed for the cause of this reflectivity. These include the mixing of crustal and mantle lithologies, ductile high-strain zones, metamorphic layering, fluid-filled cracks or high-porosity zones, and the intrusion of basaltic sills at the base of the crust (Klemperer *et al.* 1986; Meissner & Wever 1986). However, there is one important difference between the reflective lower crust in these areas and the reflective lower crust in central Tibet: the thickness of reflectivity is 40 km in Tibet. The layer is twice as thick as typical reflective lower crusts seen elsewhere (Fig. 8 and Warner 1990b) which typically begin at 12–15 km depth and have total thicknesses of 15–20 km and is thicker than the entire crust in most other regions where distinctive lower-crustal reflectivity is observed. Any explanation for the observed lower-crustal reflectivity has to explain this extreme thickness. Another important constraint is that the explanation for the lower-crustal reflectivity fits the crustal velocity model generated from the INDEPTH III refraction experiment (Zhao *et al.* 2001). Given the poor data coverage we have, the geographical extent of the reflectivity is not well controlled. However, we see enough similarities in the reflectivity from Tib 11, the Bangoin, Lumpola and Do Ma lines to postulate that a common seismic reflective character may extend from the northern end of the Yadong–Gulu Rift to Do Ma and possibly Shuang Hu, a distance of around 300 km. Any mechanism also needs to explain the possibly wide extent of this reflectivity and why this reflectivity pattern extends across the Banggong–Nujiang Suture and is seen in both the Lhasa block and Qiangtang terrane.

There are three possible scenarios for the formation of the reflective layer: (1) it was formed before or during the collision of the Lhasa and Qiangtang blocks and has been undisturbed since; (2) it is a result of deformation of a pre-existing fabric due to the Indo–Asian collision; or (3) it is a younger feature related to ongoing processes within the Tibetan Plateau today.

In the first scenario, a pre-existing fabric would be the result of intrusion of material into the lower crust during the accretion of the Lhasa block to Eurasia or before, assuming that, of the possible explanations for reflectivity mentioned above, only mafic intrusions could survive over an extended time period to produce lower-crustal reflectivity. Significant magmatic underplating and crustal intrusion occurred when the northern Lhasa Block underwent an episode of crustal melting in the Early Cretaceous (120–130 Ma) (Harris *et al.* 1990) forming a series of leucogranites which were emplaced at around 15 km (Harris *et al.* 1988) but are now exposed at the surface. One of these, the Bangoin batholith, outcrops immediately to the south of the Bangoin seismic profile. This melting episode occurred some 20 Myr after the collision that formed the Banggong–Nujiang Suture. The magmatism was concentrated south of the suture zone

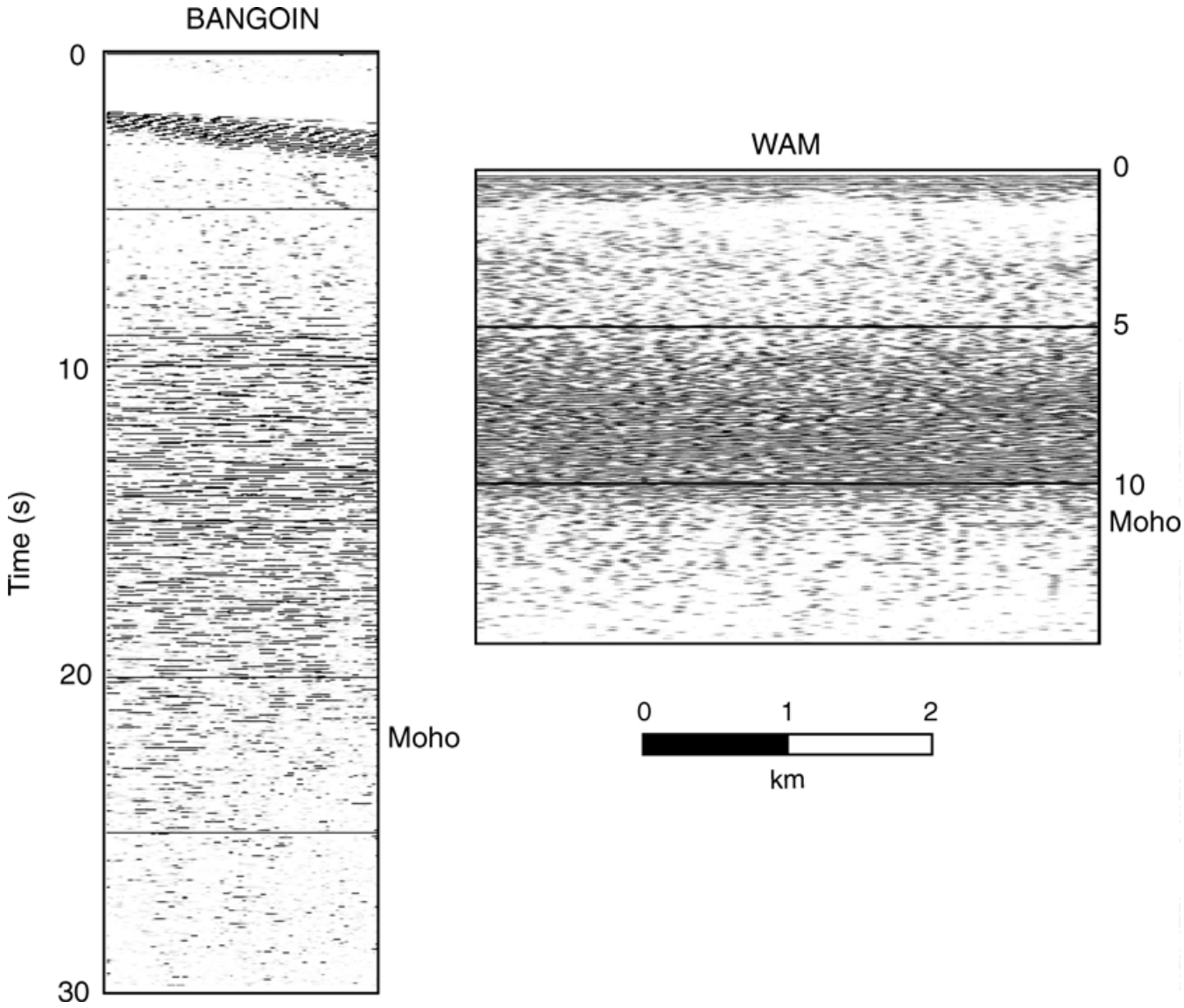

Figure 8. Comparison of INDEPTH III data from Bangoin with typical lower-crustal reflectivity from Western Europe on the BIRPS WAM line (Warner 1990a). The two lines have been aligned with the onset of the lower-crustal reflectivity. It is clear that the thickness of the reflective layer in central Tibet is much greater. The upper crust is relatively unreflective as is the upper-mantle. In both cases, the Moho is not a clear reflector but can only be identified as a termination of reflectivity.

and was not directly related to the north-dipping subduction. The Lhasa block and Qiangtang terrane were not significantly thickened immediately after the collision, with only short-lived uplift of the leucogranites and a subsequent marine transgression (Leeder *et al.* 1988). Therefore, the high temperatures required for crustal melting were produced by mantle derived melts due to post-collision lithospheric attenuation rather than crustal thickening (Harris *et al.* 1990). In order to generate the amounts of crustal melting (up to 50 per cent), the high temperatures (850 °C) and melting without the presence of water observed (Harris *et al.* 1990), significant volumes of mafic material had to have been intruded into the lower crust. This would probably produce significant lower-crustal reflectivity. However, this was a local event centred to the south of the Banggong–Nujiang Suture with the outcropping granites lying to the south of the suture zone. Hence, it cannot be used to explain lower-crustal reflectivity over a wider area unless intrusion of mafic melts occurred more generally but did not produce granites observed in outcrop. Continuity in reflectivity across the Banggong–Nujiang Suture zone could be explained if, as suggested by Yin & Harrison (2000), the lower crust of the Lhasa Block has been underthrust beneath the southern edge of the Qiangtang block. However, this scenario provides no explanation for the anomalous thickness of the reflectivity since Lhasa block crust would have had a normal thickness of 40 km to begin with (Murphy *et al.* 1997) and this region has been significantly thickened to 65 km since. Therefore, there is evidence to suggest that lower-crustal reflectivity could have existed prior to the uplift of the plateau, but it cannot be undisturbed.

Our second scenario, a deformed pre-existing fabric, is more plausible. The current thickness of the crust in this part of Tibet is 65 km with the lower crust composing some 40 km of this thickness. Murphy *et al.* (1997) suggest that the crust was originally 40 km thick. Hence, the crust has been thickened at least by 25 km. To create 65 km of crust from an original 40 km requires 38.5 per cent shortening in a pure shear model. This gives the correct modern

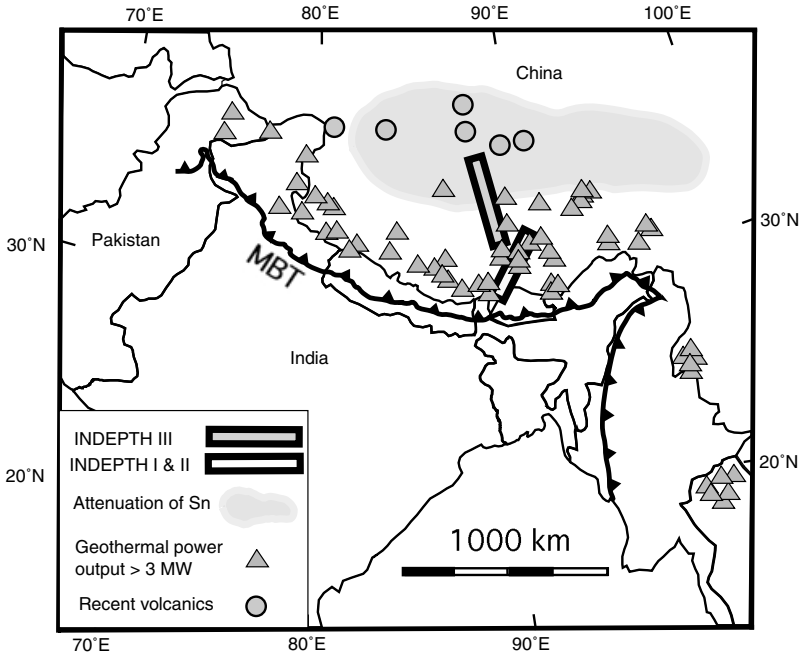

Figure 9. Location of INDEPTH profiles with respect to high energy geothermal activity >1 MW (Hochstein & Yang 1995) and upper-mantle Sn attenuation (McNamara *et al.* 1995). Attenuation of Sn has been interpreted as the result of melt in the upper-mantle.

thicknesses if the original crust was composed of 15 km upper crust and 25 km lower crust before thickening and we have no erosion. We can divide the upper and lower crust based on both the change in reflection character and an increase in velocity from 6.1 to 6.5 km s^{-1} at 30 km depth (Zhao *et al.* 2001). This velocity increase could be explained by an increase in the amount of mafic material in the middle crust consistent with the melting episode described above. However, a model with the velocity profile of normal continental crust thickened by a pure shear mechanism fits the observed crustal velocity-depth profile well (Haines *et al.* 2003) without the addition of significant amounts of mafic material in the lower crust. This argues against significant mafic contributions to the reflectivity. However, it is conceivable that significant reflectivity could be generated without affecting the average velocity of the crust at all. Therefore, it is possible that a former Lhasa block crust with a more normal thickness and reflective lower crust has produced modern, thick, lower-crustal reflectivity from stacked mafic intrusions in the lower crust. However, the limited extent of the intrusions argues against this as an explanation for the whole region of reflectivity observed.

In our third scenario the reflectivity is modern. If so what exactly is causing the reflectivity in central Tibet? One possibility is modern intrusion of mafic material. However, appreciable recent magmatic underplating is unlikely in the northern Lhasa Block and hence the southern half of the INDEPTH III profile. The mantle lid beneath this part of southern Tibet is too cold for melt from seismological observations of fast upper-mantle velocities (Barazangi & Ni 1982; McNamara *et al.* 1997) and upper-mantle earthquakes (Chen & Molnar 1983). For the Qiangtang block the story may be different. Analysis of magmatic rocks in eastern Tibet led Wang *et al.* (2001) to conclude that upper-mantle decompression melting could be occurring at present in southern Tibet. Furthermore, in the northern part of our profile, mantle-sourced melts are observed at the surface (Turner *et al.* 1993), the mantle is warmer and attenuates *S*-waves suggesting the existence of some melt (McNamara *et al.* 1995) (Fig. 9). It may be possible to have intrusions in the northern part of the profile, but probably not in the southern part. The volumes of magmatic rocks are small in the northern part so modern underplating and intrusion is unlikely to be the cause of significant regional reflectivity. Additionally, the lack of a distinct Moho reflection argues against modern underplating.

If active magmatic intrusion cannot explain the reflectivity observed, what can? The crustal velocity profile and current crustal thicknesses in central Tibet are consistent with a pure-shear thickening mechanism for the crust. Models of lower-crustal flow in Tibet (Zhao & Morgan 1987; Royden *et al.* 1997; Clark & Royden 2000) suggest that the lower crust in central Tibet is undergoing ductile flow today—a process facilitated by the development of a region of partial melt in the crust (Nelson *et al.* 1996) and the likely existence of fluids. The most likely process by which the lower crust was also thickened is by crustal flow in the past (Murphy *et al.* 1997). This flow could have thickened a pre-existing reflective layer to produce the current reflectivity with again the caveat that the Cretaceous crustal event was relatively local. However, lower-crustal flow itself can generate ductile shear structures that would give lower-crustal reflectivity. Given the evidence for lower-crustal flow today in Tibet, the lack of an anomalously high-velocity lower crust consistent with intrusions and the wide extent of the reflectivity suggests that lower-crustal flow is the most likely explanation for the observed lower-crustal reflectivity. This may also explain the difference in the reflective character of the Indian Plate on TIB 1 and the INDEPTH III lines since the Indian Plate is not undergoing ductile flow and is hence unreflective.

The reflectivity itself is therefore more likely to be produced from localized high-strain zones, high-porosity zones or even pockets of melt within a broad zone of ductile flow. Reflectivity due to lower-crustal flow may also explain the lack of a prominent Moho reflection since intrusion stopped in the Cretaceous and any prominent Moho reflector that may have been produced by underplating might have been significantly altered. The geographical limits of this

high-amplitude lower-crustal reflectivity may indicate the limits of ductile flow within the plateau. Satellite magnetic data (Alsdorf & Nelson 1999) shows that the crust below 15 km in this part of Tibet lies above the Curie temperature (∼550 °C) suggesting that the crust is hot in this region and that the weak, ductile layer should exist.

One question raised if this weak ductile layer exists in this part of Tibet is where are the bright-spots, since these were suggested to mark the level at which the lower-crustal flow becomes detached from the upper crust (Nelson *et al.* 1996). However, there may be several reasons why we do not observe bright-spots. One is that this region is hot enough to have a weak lower crust but not hot enough to form crustal melts. If the high-energy geothermal areas on the plateau correspond to the area of possible crustal melting or at least sufficient crustal fluids to support geothermal systems and hence bright-spots, part of this profile lies outside that area (Fig. 9). In fact, the existence of lower-crustal reflectivity at the northern end of TIB 11 argues for an even more limited region of melting confined to the rift zone (Fig. 7). Another possibility is that the Cretaceous melting event has dehydrated the crust to the point that no melting or metamorphic reactions can produce sufficient fluid to generate bright-spots. This does generate a problem for the creation of reflectivity. If melting removed a large amount of the fertile material from the crust and consequently the northern part of the Lhasa block is extremely dry, this rules out one possible cause of lower-crustal reflectivity, namely fluid-filled layers within a ductile flow region. A dry crust is supported by xenolith data from Hacker *et al.* (2000), albeit from 100 km north of our profiles.

Hence, the lower-crustal reflectivity cannot be simply explained as evidence for the thickening of fossil lower-crustal reflectivity almost *in situ* or by fluid-filled zones. There is rather more evidence for a modern ductile strain fabric, for three reasons. First, the flow of material in the lower crust is an explanation for the modern crustal thickness and does not depend on any other events. Second, seismic refraction data does not show an increase of seismic velocity consistent with a significant increase in mafic material in the lower crust. Third, the extent of mafic intrusion in the Cretaceous was probably not wide enough to explain all the reflectivity seen. However, the possibility that fossil fabrics may be producing at least part of the reflectivity observed cannot be entirely ruled out.

SUMMARY

Crustal scale reflection tests in central Tibet demonstrate that the crust down to the Moho can be successfully imaged. These tests have identified a thick region of lower-crustal reflectivity extending from around 25 km down to a depth of 65 km, consistent with the depth to Moho obtained by coincident refraction profiling. However, unlike southern Tibet, no crustal bright-spots have been observed. Indeed, the seismic attenuation and signal penetration in central Tibet have more in common with the Himalayas than the Yangbaijin region immediately to the south. Given the short length of the profiles collected, any interpretation of the crustal reflectivity is naturally speculative. However, the thickness of the reflective layer and the refraction velocities suggest that local thickening of the lower crust by ductile flow can explain the observations without, however, entirely ruling out the possibility that the crustal reflectivity is the result of past mafic intrusions.

ACKNOWLEDGMENTS

The authors would like to thank M. Stiller and J. Ansorge for their helpful reviews. PASSCAL provided the Geometrics reflection recording equipment. This work was supported by the Continental Dynamics Programme of the National Science Foundation and the Ministry of Mines and Geology of the People's Republic of China.

REFERENCES

Allmendinger, R.W., Nelson, K.D., Potter, C.J., Barazangi, M., Brown, L.D. & Oliver, J.E., 1987. Deep seismic reflection characteristics of the continental crust, *Geology,* **15,** 304–310.

Alsdorf, D. & Nelson, D., 1999. Tibetan satellite magnetic low; evidence for widespread melt in the Tibetan crust?, *Geology,* **27,** 943–946.

Alsdorf, D., Brown, L.D., Nelson, K.D., Makovsky, Y., Klemperer, S. & Zhao, W., 1998. Crustal deformation of the Lhasa terrane, Tibet Plateau, from Project INDEPTH deep seismic reflection profiles, *Tectonics,* **17,** 501–519.

Barazangi, M. & Ni, J., 1982. Velocities and propagation characteristics of *Pn* and *Sn* beneath the Himalayan Arc and Tibetan Plateau; possible evidence for underthrusting of Indian continental lithosphere beneath Tibet, *Geology,* **10,** 179–185.

Brown, L.D. *et al.,* 1996. Bright spots, structure, and magmatism in southern Tibet from INDEPTH seismic reflection profiling, *Science,* **274,** 1688–1690.

Chen, W. & Molnar, P., 1983. Focal depths of intracontinental and intraplate earthquakes and their implications for the thermal and mechanical properties of the lithosphere, *J. geophys. Res.,* **88,** 4183–4214.

Chen, L., Booker, J.R., Jones, A.G., Wu, N., Unsworth, M.J., Wei, W. & Tan, H., 1996. Electrically conductive crust in southern Tibet from INDEPTH magnetotelluric surveying, *Science,* **274,** 1694–1696.

Clark, M. & Royden, L., 2000. Topographic ooze: building the eastern margin of Tibet by lower crustal flow, *Geology,* **28,** 703–706.

Cogan, M.J. *et al.,* 1998. Shallow structures of the Yadong-Gulu Rift, southern Tibet, from refraction analysis of Project INDEPTH common midpoint data, *Tectonics,* **17,** 46–61.

Coward, M.P., Kidd, W.S.F., Pan Yun, Shackleton, R.M. & Zhang Hu, 1988. The structure of the 1985 Tibet Geotraverse, Lhasa to Golmud, *Phil. Trans. R. Soc. Lond.,* **327,** 307–336.

Gibson, B.S. & Levander, A.R., 1990. Apparent layering in common-midpoint stacked images of two-dimensionally heterogeneous targets, *Geophysics,* **55,** 1466–1477.

Hacker, B., Gnos, E., Ratschbacher, L., Grove, M., McWilliams, M., Sobolev, S., Jiang, W. & Wu, Z., 2000. Hot and dry deep crustal xenoliths from Tibet, *Science,* **287,** 2463–2466.

Haines, S.S., Klemperer, S., Brown, L., Guo, J., Mechie, J., Meissner R., Ross, A. & Zhao, W., 2003. INDEPTH III seismic data: From surface observations to deep crustal processes in Tibet, *Tectonics,* **22**.

Harris, N.B.W., Holland, T.J.B. & Tindle, A.G., 1988. Metamorphic rocks of the 1985 Tibet Geotraverse, Lhasa to Golmud, *Phil. Trans. R. Soc. Lond.,* **327,** 203–214.

Harris, N.B.W., Inger, S. & Xu, R., 1990. Cretaceous plutonism in central Tibet; an example of post-collision magmatism?, *J. Volc. Geotherm. Res.,* **44,** 21–32.

Hauck, M.L., Nelson, K.D., Brown, L.D., Zhao, W. & Ross, A.R., 1998. Crustal Structure of the Himalayan Orogen from Project INDEPTH Deep Seismic Reflection Profiles at ∼90°E, *Tectonics,* **17,** 481–500.

Hochstein, M.P. & Yang, Z., 1995. The Himalayan Geothermal Belt (Kashmir, Tibet, West Yunnan), in *Terrestrial Heat Flow and Geothermal Energy in Asia,* pp. 331–368, eds Gupta M.L., Yamano, M., Oxford, New Delhi.

Huang, W. *et al.,* 2000. Seismic polarization anisotropy beneath the central Tibetan Plateau, *J. geophys. Res.,* **105,** 27 979–27 989.

Kidd, W.S.F. *et al.,* 1988. Geological mapping of the 1985 Chinese–British Tibetan (Xizang–Qinghai) Plateau geotraverse route, *Phil. Trans. R. Soc. Lond.,* **327,** 287–305.

Klemperer, S.L., Hauge, T.A., Hauser, E.C., Oliver, J.E. & Potter, C.J., 1986. The Moho in the northern Basin and Range Province, Nevada, along the COCORP 40 degrees N seismic-reflection transect, *Geol. Soc. Am. Bull.,* **97,** 603–618.

Kong, X., Wang, Q. & Xiong, S., 1996. Comprehensive geophysics and lithospheric structure in the western Xizang (Tibet) Plateau, *Sci. China D,* **39,** 348–358.

Leeder, M.R., Smith, A.B. & Jixiang, Y., 1988. Sedimentology, paleoecology and paleoenvironmental evolution of the 1985 Tibet Geotraverse, Lhasa to Golmud, *Phil. Trans. R. Soc. Lond.,* **327,** 107–144.

McNamara, D.E., Owens, J.T. & Walter, W.R., 1995. Observations of regional phase propagation across the Tibetan Plateau, *J. geophys. Res.,* **100,** 22 215–22 229.

McNamara, D.E., Walter, W.R., Owens, T.J. & Ammon, C.J., 1997. Upper mantle velocity structure beneath the Tibetan Plateau from *Pn* traveltime tomography, *J. geophys. Res.,* **102,** 493–505.

Makovsky, Y. & Klemperer, S.L., 1999. Measuring the seismic properties of Tibetan bright spots: free aqueous fluids in the Tibetan middle crust, *J. geophys. Res.,* **104,** 10 795–10 826.

Makovsky, Y., Klemperer, S.L., Huang, L. & Lu, D., 1996. Structural elements of the southern Tethyan Himalaya crust from wide-angle seismic data, *Tectonics,* **15,** 997–1005.

Makovsky, Y., Klemperer, S.L., Ratschbacher, L. & Alsdorf, D., 1999. Midcrustal reflector on INDEPTH wide angle profiles; an ophiolitic slab beneath the India–Asia suture in southern Tibet?, *Tectonics,* **18,** 793–808.

Matthews, D.H. & Cheadle, M.J., 1986. Deep reflections from the Caledonides and Variscides west of Britain and comparison with the Himalayas, in *Reflection Seismology; a Global Perspective,* Vol. 13, pp. 5–19, eds Barazangi, M. & Brown, L.D., *Geodynamics Series*. AGU, Washington DC.

Meissner, R. & Wever, T., 1986. Nature and development of the crust according to deep reflection data from the German Variscides, in *Reflection Seismology; a Global Perspective,* Vol. 13, pp. 31–42, eds Barazangi, M. & Brown, L.D., *Geodynamics Series*. AGU, Washington DC.

Murphy, M. *et al.,* 1997. Did the Indo-Asian collision alone create the Tibetan Plateau?, *Geology,* **25,** 719–722.

Nelson, K.D. *et al.,* 1996. Partially molten middle crust beneath southern Tibet; synthesis of Project INDEPTH results, *Science,* **5293**.

Owens, T.J. & Zandt, G., 1997. Implications of crustal property variations for models of Tibetan Plateau evolution, *Nature,* **387,** 37–43.

Rapine, R., Rogers, A., Tilman, F. & Ni., J., 2000. Differences in the crustal structure of Northern and Southern Tibet from surface wave dispersion and regional waveform modeling, *EOS, Trans. Am. geophys. Un. Fall Meeting Suppl.,* **81,** F1091.

Ross, A.R., Brown, L.D., Alsdorf, D.E. & Nelson, K.D., 2003. Deep seismic bright spots and magmatism in southern Tibet, *J. geophys. Res.,* in press.

Royden, L.H., Burchfiel, B.C., King, R.W., Wang, E., Chen, Z., Shen, F. & Liu, Y., 1997. Surface deformation and lower crustal flow in eastern Tibet, *Science,* **276,** 788–790.

Sapin, M., Wang, X.J., Hirn, A. & Xu, Z.X., 1985. A seismic sounding in the crust of the Lhasa Block, Tibet, *Ann. Geophys.,* **3,** 637–646.

Sheriff, R.E. & Geldart, L.P., 1987. *Exploration Seismology,* Vol. 2, Cambridge University Press, Cambridge.

Steer, D.N., Knapp, J.H., Brown, L.D., Echtler, H.P., Brown, D.L. & Berzin, R., 1998. Deep structure of the continental lithosphere in an unextended orogen; an explosive-source seismic reflection profile in the Urals (Urals Seismic Experiment and Integrated Studies (URSEIS 1995)), *Tectonics,* **17,** 143–157.

Turner, S., Hawkesworth, C., Liu, J., Rogers, N., Kelley, S. & van Calsteren, P., 1993. Timing of Tibetan uplift constrained by analysis of volcanic rocks, *Nature,* **364,** 50–54.

Wang, J., Yin, A., Harrison, T.M., Grove, M., Zhang, Y. & Xie, G., 2001. A tectonic model for Cenozoic igneous activities in the eastern Indo-Asian collision zone, *Earth planet. Sci. Lett.,* **188,** 123–133.

Warner, M., 1987. Migration; why doesn't it work for deep continental data?, *Geophys. J. R. Astron. Soc.,* **89,** 21–26.

Warner, M.R., 1990a. Absolute reflection coefficients from deep seismic reflections, *Tectonophysics,* **173,** 15–23.

Warner, M.R., 1990b. Basalts, water, or shear zones in the lower continental crust?, *Tectonophysics,* **173,** 163–174.

Wei, W. *et al.,* 2001. Widespread fluids in the Tibetan crust, *Science,* **292,** 716–718.

Yin, A. & Harrison, T.M., 2000. Geologic evolution of the Himalayan–Tibetan orogen, *Ann. Rev. Earth Planet. Sci.,* **28,** 211–280.

Yuan, X., Ni, J., Kind, R., Mechie, J. & Sandvol, E., 1997. Lithospheric and Upper-mantle Structure of Southern Tibet from a seismological passive source experiment, *J. geophys. Res.,* **102,** 27 491–27 500.

Zhao, W.-L. & Morgan, W.J.P., 1987. Injection of Indian crust into Tibetan lower crust; a two-dimensional finite element model study, *Tectonics,* **6,** 489–504.

Zhao, W. *et al.,* 1993. Deep seismic reflection evidence for continental underthrusting beneath southern Tibet, *Nature,* **366,** 557–559.

Zhao, W. *et al.,* 2001. Crustal structure of central Tibet as derived from project INDEPTH wide-angle seismic data, *Geophys. J. Int.,* **45,** 486–498.